Macroporous high-temperature insulators physical properties by *in situ* CA_6 formation: does the calcium source matter?

O.H. Borges [1,2,*]; T. Santos Junior [1,2]; R. R. B. Oliveira [2]; V. R. Salvini [3]; V.C. Pandolfelli [1,2]

(1) Federal University of Sao Carlos, Graduate Program in Materials Science and Engineering.

(2) Materials Microstructure Engineering Group (GEMM), FIRE Associate Laboratory, Federal University of São Carlos, Materials Engineering Department, Rodovia Washington Luis, km 235, São Carlos, SP, 13565-905, Brazil.

(3) College of Technology (FATEC), Jordão Borghetti Street 480, Sertãozinho, SP, 14160-050, Brazil

*Corresponding author at: +55-16-33518253; fax: +55-16-33615404.

E-mail: mailto:otavio.borges@dema.ufscar.br

Abstract

Aiming the *in situ* formation of CA_6 ($CaO{\cdot}6Al_2O_3$) at alumina-based macroporous insulators, distinct Ca^{2+} sources and contents were used and their effect on some of the refractories properties were investigated. Adding $CaCO_3$, $Ca(OH)_2$ or CaO resulted in the decrease of the strengthening onset temperature (T_S) and also of the linear shrinkage. However, a higher amount of $Ca(OH)_2$ and CaO could not be used because of their effect on reducing the insulator total porosity. The composition prepared with 12.9wt% of $CaCO_3$ was the most promising one, leading to an expansion of 0.81% after firing at 1600ºC for 5h, T_S of 680ºC and low thermal conductivity. These results point out the potential reduction of sintering temperatures and to the possibility of *in situ* firing the ceramic insulator. These features enable the development of a macroporous refractory composition with a higher thermal insulating effectiveness, which can help industries to decrease their energy demand.

Keywords: Calcium sources, Macroporous insulators, Direct foaming, Linear shrinkage.

DOI: 10.1016/j.jeurceramsoc.2020.04.001

1. Introduction

Constant efforts are being made aiming at cost reduction in all economic sectors. Due to the strong competition, the industries are even more susceptible to this scenario and to cope with that, heavy investments in research and development of new materials and processes are required [1]. Energy-related costs are one of the most relevant for industries, especially for those operating at high temperatures (>1000 °C) [2]. Such industries are called energy-intensive and were responsible for 12% of all energy consumed in 2018 [2].

In this context, macroporous refractory ceramics have been drawing attention as they can be used as thermal insulators, reducing the amount of energy demanded and decreasing production costs. However, some challenges should be overcome to increase macroporous ceramics applications. Among them, the control of shrinkage after firing and the reduction of thermal conductivity can be cited. Additionally, for macroporous insulators produced by direct foaming methods, the control of aging phenomena, which take place before foam solidification, is another key issue. These phenomena act by increasing the average size of bubbles and making their distribution wider [3], which makes it more difficult to achieve the target microstructure designed for the thermal insulator.

Regarding the reduction of shrinkage after firing, a promising alternative could be the *in situ* formation of expansive phases, such as hibonite (also known as calcium hexaluminate, $CaO{\cdot}6Al_2O_3$, or just CA_6), which induces a significant volumetric expansion due to its low density and asymmetrical crystals [4,5]. Thus, this expansive effect due to CA_6 formation could counteract the material shrinkage. Furthermore, plain CA_6 presents high refractoriness, incongruent melting close to 1800 ºC [6] (however, impurities source and content can reduce this refractoriness significantly) and low thermal

conductivity, so its incorporation as light aggregate in thermal insulators has already been tested, inducing significant reductions in their effective thermal conductivity. [7,8].

Distinct Ca^{2+} sources can be used to produce CA_6 *in situ* [6], such as calcined calcium oxide (CaO), calcium carbonate ($CaCO_3$), calcium hydroxide [$Ca(OH)_2$] and calcium aluminate cement (CAC). Besides promoting CA_6 formation when heated up to 1400 ºC in the presence of Al^{3+} sources, recent studies have shown that $CaCO_3$ and $Ca(OH)_2$ induced lower strengthening temperature in dense alumina-based refractories when compared to samples containing just CAC as Ca^{2+} source [9,10], as can be seen in Figure 1.

Figure 1

Therefore, using these Ca^{2+} sources in alumina-based macroporous refractories is of great technological interest as the material could be thermally treated at lower temperatures to be applied in low thermal demand environment (e.g. in aluminum industries) or to attain enough mechanical strength for transportation and installation, finishing their firing process *in situ*. In both cases, energy and natural resource savings would be achieved. Additionally, depending on the amount of CA_6 formed after the thermal treatment, it can be able to completely counteract the shrinkage of the refractory leading to its expansions, which can result in a more effective joint closure as the material stays under some mild compressive stress. However, the temperature gradient should be controlled to avoid thermal spalling.

However, the impact of each Ca^{2+} source on the material properties (such as mechanical strength, shrinkage, elastic modulus, porosity, pore size distribution, and the effective thermal conductivity) is not yet completely understood and was investigated in this work.

2. Materials and methods

2.1 Materials

Macroporous samples were produced using a standard composition (see Table 1) and a direct foaming method [11], which consisted of incorporating a previously prepared surfactant-based foam into an alumina suspension, as described in [12]. Alumina CL370 and CT3000SG (Almatis, Germany) were used in the appropriate ratio to obtain optimized packaging, according to Andreasen's model (q=0.37). These raw materials were dispersed in distilled water, containing the dispersive agent Castament® FS 60 (BASF, Germany) and a commercial non-ionic surfactant based on alkyl-polyethylene-glycol-ether (Lutensol® AT 50 Pulver, BASF, Germany). To obtain the foam, which was produced incorporating air into a liquid phase by mechanical stirring, a commercial surfactant based on 1,2-benzoathiazolin-3(2h)-one (Vinapor GYP 2680, BASF, Germany) and a thickening agent comprised by Hydroxietil Celulose (Cellosize 100 CG FF, Dow Chemical, USA) were used.

Table 1: Basic composition for the ceramic foam

Ceramic foam composition		
	Raw materials	**wt%**
Al_2O_3 Suspension	CL370	76.06
	CT3000SG	5.72
	FS60	0.09
	Lutensol AT50	0.10
	Water	15.79
Foam	Vinapor	3.468
	Hydroxietil Celulose	0.0056

Thereby, all formulations were produced using the standard composition described in Table 1 and each of them distinguished themselves by the type and amount of the Ca^{2+} source used. It is worth observing that the Ca^{2+} content was adjusted for each

composition, such as the amount of CA_6 formed after the thermal treatment was the same. Table 2 shows the nomenclature code used, as described below:

"Percentage indicating the theoretical CA_6 content formed after firing"_"main Ca^{2+} source"/"secondary Ca^{2+} source" (when it was used)

Hydratable alumina (Alphabond 300, Almatis, Germany), calcium oxide (CaO, D50 = 14.56 μm, obtained by calcination of calcium carbonate at 900 ºC for 4 hours) and calcium aluminate cement (Secar 71, Imerys Aluminates, France) as a powder or as stable aqueous suspension (produced as described in [13]) were the binders. Besides those, commercial calcium carbonate (Imerys, France, 99% purity, D_{10} = 1.49 μm, D_{50} = 7.38 μm, D_{90} = 12.64 μm) and calcium hydroxide [$Ca(OH)_2$, Synth, Brazil, 99.9% purity, D_{10} = 2.76 μm, D_{50} = 5.66 μm , D_{90} = 11.00 μm] were also used as Ca^{2+} sources. Table 3 shows the additives added for each composition. The Ca^{2+} precursors used in this paper are of high purity to ensure better experimental parameter control.

Table 2: Abbreviations used in the nomenclature system of the samples.

Ca^{2+} Source	
Name	Abbreviation
Calcium carbonate	$CaCO_3$
Calcium aluminate cement	S71
Calcium hydroxide	$Ca(OH)_2$
Stable S71 aqueous suspension	CAC_L
Calcium oxide	CaO

Table 3: Ca^{2+} sources and contents for each composition.

		Additive (wt%)				
		Secar 71	α-Bond	$CaCO_3$	$Ca(OH)_2$	CaO
Composition	REF.	-	1.00	-	-	-
	20_S71	5.00	-	-	-	-
	20_CAC_L	5.00	-	-	-	-
	20_$CaCO_3$/S71	1.00	-	2.04	-	-
	20_$Ca(OH)_2$/S71	1.00	-	-	1.55	-
	20_CaO	-	-	-	-	1.42
	40_$CaCO_3$/S71	1.00	-	4.55	-	-
	40_$Ca(OH)_2$/S71	1.00	-	-	2.60	-
	40_CaO	-	-	-	-	2.82
	80_$CaCO_3$/S71	1.00	-	10.02	-	-
	80_$Ca(OH)_2$/S71	1.00	-	-	5.72	-
	80_CaO	-	-	-	-	5.86
	100_$CaCO_3$/S71	1.00	-	12.90	-	-

Cylinders (50 mm x 50 mm and 40 mm x 40 mm), bars (150 mm x 25 mm x 25 mm) and bricks (230mm x 114mm x 64mm) were produced as samples. For compositions containing S71 or CAC_L, the curing step took place in a climatic chamber (VC 2020, Vötsch, Germany) at 50ºC and relative humidity of 80% for 24 hours. For the other compositions, curing was carried out at 50ºC for 24 hours, without humidity control. All samples were dried at 110ºC for 24 hours and, after this process, they were classified as "green". Additionally, some of these green samples were submitted to a thermal treatment of up to 1600 ºC for 5 h to enable strengthening and complete CA_6 formation. These samples were classified as "fired".

2.2 Methods

The compositions were evaluated according to their linear shrinkage after firing and total porosity using a relationship between the porous sample density (liquid

immersion method, based on the Archimedes' principle, according to ASTM C20 [14]) and the density of the solid fraction [measured by helium pycnometry (AccuPyc 1330, Micromeritics, USA) of the powder obtained by grinding the samples]. Cold crushing strength was carried out in MTS 810 equipment (MTS, USA), according to ASTM C133 [15]. Pore size distribution was evaluated by image analysis obtained from a stereomicroscope Stemi 2000-C, coupled to an AxioCam ERc5S camera (both from Zeiss, Germany) and using the Software Digimizer® (version 5.1.2, MedCalc Software bv). The mineralogical phase content of each composition after firing was analyzed applying the Rietveld refinement method (software Topas, Bruker, USA) based on X-ray diffractograms (Geiger-Flex diffraction, Rigaku, Japan), ensuring Goodness of Fit (GOF) < 1.5 and weighted profile R-factor (RWP) < 15 %. Sinterability was *in situ* monitored by tracking the elastic modulus versus temperature profile up to 1400 ºC using Sonelastic equipment (ATCP Physical engineering, Brazil), according to ASTM E1875 [16]. Thermal conductivity as a function of temperature up to 1200 °C was evaluated by the parallel hot wire technique (according to ASTM C1113 [17]), in TCT 426 equipment (Netzch, Germany). Additionally, some selected compositions' microstructures were analyzed after firing by scanning electron microscopy (SEM) in an XL-30 FEG microscope (Philips, Amsterdam) using the backscattered electron mode (BSE).

3 Results and discussion

3.1 Effect of distinct Ca^{2+} sources on some properties of alumina-based macroporous thermal insulators

To evaluate the effect of using distinct Ca^{2+} sources in alumina-based macroporous insulators, compositions REF, 20_S71, 20_CAC_L, 20_$CaCO_3$/S71, 20_$Ca(OH)_2$/S71 and 20_CaO were characterized by their linear shrinkage and total porosity at green and fired conditions (Figure 2). All compositions presented total green

porosity above 75%, highlighting the effectiveness of using a direct foaming method with an organic surfactant to produce high-porosity macroporous insulators. After the thermal treatment (1600 ºC for 5h), a clear trend of porosity decrease can be noticed. This result is due to the densification, which acts closing pores and leading to shrinkage. Just for composition 20_CaO, this effect could not be seen, however, if the standard deviations were considered, it is possible that even for this composition the total porosity after firing has been reduced.

Figure 2

Nevertheless, the total fired porosity for all compositions containing Ca^{2+} was above 75 vol%, whereas for composition REF (which had no Ca^{2+} source added) this value was below 65 vol%. The significant reduction in the total porosity showed by composition REF can be explained by its higher linear shrinkage (close to 12%) compared to the others (ranging from 6.5% to 8%). The lower shrinkage presented by Ca^{2+}-containing compositions is assigned to CA_6 formation after the thermal treatment at 1600ºC for 5h. Additionally, as the shrinkage values of these compositions were not statistically distinct, it can be assumed that the amount of CA_6 formed was equivalent.

Another key property for a macroporous insulator is its pore size distribution, which affects both mechanical strength and thermal conductivity at high temperatures [18–20]. Regarding the latter, some computational studies pointed out that pore sizes ranging from 3 μm to 0.5 μm are the ideal to interact and spread the thermal radiation at high temperatures (1000ºC – 2000ºC) [20]. The pore size distribution of the aforementioned compositions can be seen in Figure 3. Initially, it is worth observing that none of them presented a significant fraction of pores within the ideal range, which shows that the processing conditions used were not able to produce and/or stabilize bubbles of

such sizes [3]. Using more efficient equipment to produce and reduce the size of bubbles – as developed by Salvini *et al.* [7] – or a more effective bubble stabilizing system – e.g. functionalized particles or proteins [21] – would be alternatives to increase the pore fraction between 3µm and 0.5 µm.

Composition 20_$Ca(OH)_2$/S71 presented the smallest and narrowest pore size distribution that can be associated to a slightly viscosity increase attained for the alumina suspension containing calcium hydroxide, which slows the aging phenomena of foams underwent before setting [22]. This behavior can be explained by the plate-shaped geometry of $Ca(OH)_2$ particles, which affects the system's rheology, resulting in a pseudoplastic suspension [23]. An analogous result could be seen for composition 20_CaO, which presented the second narrowest pore size distribution. Due to the presence of CaO, which has a fast reaction kinetics with water [24], the liquid foam in this composition displayed a quick increase in its viscosity. Therefore, CaO acted as a quick-setting binder, reducing the time that aging phenomena could act on the liquid foam.

Composition 20_$CaCO_3$/S71 and REF showed equivalent pore size distribution, highlighting that the Ca^{2+} sources used in this composition had little effect on this property. On the other hand, those containing just CAC, both as powder (20_S71) and as aqueous suspension (CAC_L), presented wider pore size distribution, with an increase of the larger pores. In both cases, the addition of CAC resulted in the partial destabilization of the foam, which speeds up the aging phenomena.

Figure 3

These formulations were also evaluated by their cold crushing strength (Table 4). Composition REF presented the highest value of mechanical strength both at green and fired conditions. For the former, the effectiveness of hydratable alumina as a hydraulic

binder was determinant. However, the highest values achieved by fired samples can be attributed to the lower porosity of composition REF, based on the high densification undergone by this composition, as shown in Figure 2.

Table 4: Cold crushing strength of green (110 ºC for 24 h) and fired (1600 ºC for 5 h) samples with distinct Ca^{2+} sources.

Compositions	Crushing strength of green samples (MPa)	Crushing strength of fired samples (MPa)
REF	0.95 ± 0.03	62 ± 2
20_S71	0.065 ± 0.006	2.2 ± 0.2
20_CAC_L	0.75± 0.04	4.7 ± 0.5
20_$CaCO_3$/S71	0.51 ± 0.04	7.4 ± 0.4
20_$Ca(OH)_2$/S71	0.060 ± 0.004	4.2 ± 0.4
20_CaO	0.096 ± 0.007	4.2 ± 0.5

The main advantage of using CAC as aqueous suspension instead of powder can be seen by comparing the green mechanical strength of compositions 20_S71 to 20_CAC_L. The former showed the lowest value observed, whereas 20_CAC_L stood out presenting the second highest. Therefore, even though both compositions had equivalent cement content and porosity level, the use of CAC as aqueous suspension enabled better dispersion of cement particles in the foam structure, leading to a more effective mechanical reinforcement.

Compositions 20_S71, 20_$Ca(OH)_2$/S71 and 20_CaO presented equivalent green mechanical strength, however, composition 20_$CaCO_3$/S71 showed strength values closer to that of 20_CAC_L. This behavior can be explained by the dispersing effect that calcium carbonate can induce to cement [25]. Therefore, it is additional evidence that better CAC dispersion plays a key role in the mechanical strength of green samples.

Whereas the green mechanical strength is mainly affected by the effectiveness of the binding system, after firing this property relies on the resulting mineralogical phases and how they are spatially organized and bounded. In this regard, composition 20_S71 showed the lowest fired cold crushing strength, followed by 20_CaO, 20_$Ca(OH)_2$/S71 and 20_CAC_L – that presented intermediate values –, and 20_$CaCO_3$/S71, which achieved the highest one. This sequence of mechanical strength values can be explained by the morphology of the formed CA_6 that could be asymmetric or equiaxial [26,27]. Therefore, for 20_S71 composition, CA_6 very has likely been formed with a lower aspect ratio, whereas the other formulations' (whose microstructure is presented in Figure 6) elongated CA_6 grains were obtained. Indeed, it is reported in the literature that the use of non-oxide Ca^{2+} sources induces the formation of the higher aspect ratio CA_6 [6,26].

Considering the phenomenon reported by Luz *et al.* [10], the effect of Ca^{2+} sources on the mechanical strengthening of each composition during the thermal treatment was evaluated by measuring the elastic modulus as a function of temperature during the firing process from room temperature up to 1400 ºC. The results achieved can be seen in Figure 4. Firstly, it was observed that all compositions presented a green Young's modulus ranging from 0.85 GPa to 1.3 GPa. The heating step up to 500 ºC resulted in the decrease of these values due to hydroxilated phases decompositions, such as boehmite [$Al(OH)_3$], portlandite [$Ca(OH)_2$] and the hydrates formed by cement.

However, the effect of some Ca^{2+} sources on the strengthening temperature (T_S) stood out. For compositions REF, 20_S71 and 20_CAC_L, T_S was in the range of 900 ºC and 915 ºC, whereas the use of other Ca^{2+} sources decreased this value to ~ 690 ºC. These results indicated that adding calcium aluminate cement, either as powder or as aqueous suspension, does not bring benefits in terms of reducing the strengthening temperature. On the other hand, calcium carbonate, calcium hydroxide and calcium oxide were able to

decrease this temperature closer to 700ºC, which are in accordance with the results presented by Consoni *et al.* for dense alumina-based refractory systems [9].

Figure 4

This Young´s modulus (E) increase at lower temperatures is technologically interesting because it can enable the material to be thermally treated at lower temperatures, allowing its transportation and installation, finishing their firing process *in situ*. Therefore, this phenomenon may result in a significant reduction of energy input required to manufacture macroporous thermal insulators. Besides that, using lower sintering temperatures to manufacture porous thermal insulators that should be applied in low thermal demand environments (e.g. in aluminum industries) is an extra benefit. In both cases, significant energy and natural resource savings would be achieved.

Additionally, considering that 40 % of the CO_2 emitted by the production of cement results from the combustion of fuels in the kiln [28] (which work at ~ 1500 ºC [29]), the replacement of CAC by $CaCO_3$, $Ca(OH)_2$ or CaO can reduce the carbon footprint and the embodied energy of the refractory thermal insulators. That is because the combustion of fuels in the kiln is avoided in case of using $CaCO_3$ (which is available in nature) and is reduced when CaO or $Ca(OH)_2$ is used (as the former is produced by the calcination of $CaCO_3$ up to 1000 ºC, and the latter is obtained by the hydration of calcined CaO).

The results discussed so far indicate that samples with $CaCO_3$, $Ca(OH)_2$ and CaO are more promising for the production of CA_6 and reduction of T_S than those containing only CAC or without Ca^{2+} sources. Those compositions presented higher total porosity, lower linear shrinkage, narrower pore size distribution with a smaller average size value (D_{50}), suitable mechanical strength and, finally, lower strengthening temperature (T_S). Thus, aiming to overcome some of the challenges previously mentioned, compositions

containing higher Ca^{2+} content from these three sources [$CaCO_3$, $Ca(OH)_2$ and CaO] were produced and some of their additional properties have been evaluated.

3.2 Characterization of Al_2O_3-based refractory macroporous ceramics with increased amount of Ca^{2+}.

Figure 5 shows linear shrinkage and total porosity for each composition both at green and fired conditions. The increase of $CaCO_3$ content did not significantly affect the material's total porosity, however the addition of $Ca(OH)_2$ and CaO in higher concentrations (to result in 80 wt% or more of CA_6 after firing) induced a significant porosity decrease. Therefore, it was not possible to produce such compositions by the route and quantities used in this work and described in session 2.1, as the porosity in these compositions was lower 50%. This phenomenon was attributed to the high viscosity increase that these Ca^{2+} sources promote, either by the quick-hydration of CaO or the rheological changes induced by $Ca(OH)_2$. Therefore, this viscosity increase favored the increase of porosity in compositions with 20% and 40% of theoretical CA_6-content, but not in the ones with even higher contents of $Ca(OH)_2$ or CaO. This behavior was expected, as there is an optimum range of viscosity to stabilize bubbles, as shown by Mao [22]. If in on hand low viscosity values make aging phenomena act more intensely, on the other hand, high viscosity values hamper the incorporation of air bubbles into the alumina-based suspension [22,30]. However, even though this optimum range of viscosity varies for each system, a value around 0.1 Pa s – which is 100 times the viscosity of water – is indicated in the literature as appropriate to decrease the action of aging phenomena without halting foamability [30].

Besides that, it is worth noticing that composition 80_$CaCO_3$/S71 underwent almost no shrinkage and composition 100_$CaCO_3$/S71 presented a linear expansion of ~1% after the thermal treatment at 1600 ºC for 5 h and, additionally, their total porosity

remained close to 80 %. Therefore, the CA_6 formation was able to counteract the shrinkage of the material, leading even to its expansion. This behavior can result in a more effective joint closure if the insulator was sintered *in situ*, leaving the material under some compressive stress, which is of great technological interest.

Figure 5

The $CaCO_3$-containing compositions always presented lower shrinkage when compared to those containing the same Ca^{2+} content but prepared with $Ca(OH)_2$ and CaO (see Figure 5), which can be attributed to a higher aspect ratio CA_6 induced by using $CaCO_3$, leading to a larger volumetric expansion [6]. The microstructure of compositions containing these three Ca^{2+} sources (prefix 20) can be seen in Figure 6, where the effect of $CaCO_3$ in the CA_6 morphology can be noticed. In all cases, hibonite seems to be formed in tabular shape whereas 20_$CaCO_3$/S71 shows the large (highly asymmetric) crystals, 20_$Ca(OH)_2$ exhibits thin tabular grains partially aggregated, and 20_CaO displays very equiaxial grains.

Figure 6

Additionally, the linear shrinkage and designed CA_6 content of each set of compositions presented a linear variation, which can be represented by Eq. 1 (derivative using the method of least squares and valid for the CA_6 amount between 20 wt% and 100 wt%). This equation can forecast the desired linear shrinkage/expansion of the studied systems by adjusting the type and content of the Ca^{2+} source. It is worth noticing that R^2 is higher than 0.96 for all systems, indicating the good fitness of Eq. 1.

$$\text{Linear Shrinkage} = a \cdot (\text{CA}_6 \text{ expected content}) + b \qquad \text{(Eq.1)}$$

Where a, b and R^2 for each set of compositions are presented in Table 5.

Table 5: Values of a, b and R^2 for linear regression equation that correlates CA_6 content and shrinkage after firing at 1600 ºC for 5 h.

System	*a*	*b*	R^2
$CaCO_3$/S71	-0.093	8.008	0.966
$Ca(OH)_2$/S71	-0.107	9.555	0.998
CaO	-0.088	9.570	0.996

The cold crushing strength of each composition was also evaluated – both at green and fired conditions – and the results are presented in Figure 7. Compositions of the $CaCO_3$/S71 system did not present a significant variation on mechanical strength when calcium carbonate content was increased. On the other hand, composition 80_CaO showed an important increase of mechanical strength when compared to the other compositions of the CaO system, which was associated to its porosity decrease, as previously discussed. Thus, composition 80_CaO, despite presenting a higher mechanical strength, should not be an efficient thermal insulator due to its relatively low porosity.

Figure 7

Other key properties to characterize these distinct formulations were evaluated and are shown in Table 6. All compositions had onset strengthening temperature (T_S) around 700 ºC and increments in the Ca^{2+} content resulted in a slight decrease of T_S. Besides that, it is worth noticing that a high amount of hibonite could be obtained in some compositions, which is of interest as this phase presents low thermal conductivity, high thermal shock resistance and volumetric expansion when produced *in situ*, all desired properties for a thermal insulator [5,8]. Additionally, the amount of CA_6 designed and that obtained after firing was very close, highlighting that the thermal treatment at 1600 ºC for 5h was enough to achieve the phase equilibrium, which brings further chemical and dimensional stability to the material during its use.

Table 6: Onset strengthening temperature, CA_6 content attained and D_{50} of the pore size distribution for compositions of $CaCO_3$/S71, $Ca(OH)_2$/S71 and CaO systems.

Compositions	Onset strengthening temperature (ºC)	CA_6 attained after the thermal treatment (wt %)	D_{50} of pore distribution (µm)
20_$CaCO_3$/S71	700	20.4	115
20_$Ca(OH)_2$/S71	700	19.7	55
20_CaO	685	19.6	77
40_$CaCO_3$/S71	695	40.1	93
40_$Ca(OH)_2$/S71	695	39.8	54
40_CaO	685	38.6	98
80_$CaCO_3$/S71	690	79.9	113
80_$Ca(OH)_2$/S71	690	79.7	72
80_CaO	680	77.8	124
100_$CaCO_3$/S71	680	99.1	142

Regarding the average pore size distribution (D_{50}), the increase of Ca^{2+} content – above a certain value – resulted in a rise of D_{50}. However, this critical content, which is related to the increase in viscosity induced by the increment of the Ca^{2+} sources, was distinct for each system. Formulations in the $CaCO_3$/S71 system just presented an increase of D_{50} for a composition with prefix "100", whereas formulations in the $Ca(OH)_2$/S71 and CaO ones underwent this phenomenon for compositions with prefixes "80" and "40", respectively. These results reinforce the unfeasibility of using the systems $Ca(OH)_2$/S71 and CaO to obtain a full CA_6 macroporous material, without negatively affecting some key properties for a thermal insulator (e.g. total porosity and pore size distribution).

Finally, composition 100_$CaCO_3$/S71, which showed the most promising set of results among the other compositions tested (e.g. expansion after firing, high porosity and high CA_6 content), was evaluated according to its effective thermal conductivity (k_{eff}) at temperatures ranging from 40 ºC to 1200 ºC. The obtained results, as well as values

reported by macroporous ceramics (with or without pre-fabricated CA_6 lightweight aggregates) [7] and data from a commercial alumino-silicate fiber mats with a bulk density of 103 kg m^{-3} [31], can be seen in Figure 8.

Figure 8

Composition 100_$CaCO_3$/S71 showed lower k_{eff} than the macroporous ceramic containing just Al_2O_3, however, compared to the fiber-based insulator, it presented higher k_{eff} at low temperatures (< 1000 ºC). Nevertheless, because its microstructure is not able to effectively interact with the thermal radiation emitted at high temperatures, the fiber-based material underwent a more significant increase of k_{eff}. Thus, above 1000 ºC, composition $CaCO_3$/S71 presented lower k_{eff} than the fiber-based insulator.

Additionally, composition 100_$CaCO_3$/S71 and the macroporous insulator containing 75 wt% of CA_6-based lightweight aggregates showed equivalent k_{eff} at the temperature range analyzed, highlighting the effect of hibonite on the insulators' thermal conductivity. However, it is worth noticing that besides rising production costs, the use of CA_6 as raw material does not provide the counteraction effect of densification-driven shrinkage nor the reduction of onset strengthening temperature.

4 Conclusions

The effects of adding distinct Ca^{2+} sources in alumina-based macroporous insulators produced by a direct foaming method were evaluated. $CaCO_3$, $Ca(OH)_2$ and CaO were able to induce reductions on the onset strengthening temperature (T_S), which was not detected using calcium aluminate cement (neither as a powder nor as a stable aqueous suspension). The results indicate that they can be applied to lower the firing temperatures used in the production of macroporous materials, leading to the reduction

of processing energy. Additionally, the replacement of CAC by $CaCO_3$, $Ca(OH)_2$ or CaO can also abate the carbon footprint of these thermal insulators.

Besides that, all Ca^{2+} sources tested were effective at inducing the *in situ* formation of CA_6 after thermal treatment at 1600 ºC for 5 h. However, due to their impact on the system rheology, CaO and $Ca(OH)_2$ were not feasible to be used in higher contents as they reduced the porosity and increased the pore size. On the other hand, $CaCO_3$ could be added in higher concentrations, favoring the production of a composition comprising 100% of CA_6 (named 100_$CaCO_3$/S71). The expansive effect due to CA_6 formation indeed counteracted the materials shrinkage up to 1600 ºC and a first-order trend between the dimensional change and the designed CA_6 content could be described by a linear equation. Furthermore, linear expansion of almost 1% was observed for composition 100_$CaCO_3$/S71, which is of technological interest, as a more efficient closure of the refractory lining joint can be attained in case of firing the insulator *in situ*. However, the first heating should be slow enough to avoid thermomechanical spalling.

Therefore, this expansive behavior added to its high porosity (80 %), feasible mechanical strength for manufacturing and handling, low T_S (680 ºC) and k_{eff} (0.62 W m^{-1} K^{-1} at 1200 ºC) made composition 100_$CaCO_3$/S71 the most promising among the others and its application can increase the thermal efficiency of high temperature processes, lowering environmental impacts and production costs. However, some properties could be improved to achieve even better performance, as narrower pore size distribution, higher mechanical strength and CA_6 formation at lower temperatures can be adjusted.

5 Acknowledgments

This study was financed in part by the Coordenação de Aperfeiçoamento de Pessoal de Nível Superior - Brazil (CAPES) - Finance Code 001; by the Conselho Nacional de Desenvolvimento Científico e Tecnológico – Brazil (CNPq) – Process 130843/2018-0; and by Fundação de Amparo à Pesquisa do Estado de São Paulo – Brazil (FAPESP) – Process 2018/07745-5. Additionally, the authors are thankful to BASF Construction Solutions GmbH, to RHI Magnesita and to FIRE – International Federation for Refractory Research and Education.

6. References

[1] V. Staack, R. Moebius, How companies can improve innovation, reduce costs, and mitigate risk, Strategyand - PwC, 2015. https://www.strategyand.pwc.com/media/file/Strategic-product-value-management.pdf.

[2] G. Schierning, Bring on the heat, Nat. Energy. 3 (2018) 92–93. doi:10.1038/s41560-018-0093-4.

[3] I. Cantat, S. Cohen-Addad, F. Elias, F. Graner, R. Höhler, O. Pitois, F. Rouyer, A. Saint-Jalmes, R. Flatman, Foams: structure and dynamics, Oxford University Press, 2013. doi:10.1093/acprof:oso/9780199662890.001.0001.

[4] Y. Li, R. Xiang, N. Xu, Q. Wang, S. Li, M. Wu, C. Yang, Fabrication of calcium hexaluminate-based porous ceramic with microsilica addition, Int. J. Appl. Ceram. Technol. 15 (2018) 1054–1059. doi:10.1111/ijac.12868.

[5] J. Sakihama, R. Salomão, Microstructure development in porous calcium hexaluminate and application as a high-temperature thermal insulator: a critical review, Interceram - Int. Ceram. Rev. 68 (2019) 58–65. doi:10.1007/s42411-019-0034-7.

[6] R. Salomão, V.L. Ferreira, I.R. de Oliveira, A.D.V. Souza, W.R. Correr, Mechanism of pore generation in calcium hexaluminate (CA_6) ceramics formed *in situ* from calcined alumina and calcium carbonate aggregates, J. Eur. Ceram. Soc. 36 (2016) 4225–4235. doi:10.1016/j.jeurceramsoc.2016.05.026.

[7] V.R. Salvini, A.P. Luz, V.C. Pandolfelli, Foam sprayed porous insulating refractories, Refract. Worldforum. 4 (2012) 93–97.

[8] V.R. Salvini, A.P. Luz, V.C. Pandolfelli, High temperature Al_2O_3 - CA_6 insulating foamed ceramics: processing and properties, Interceram - Refrac. Man. 59 (2012) 335–339.

[9] L.B. Consonni, A.P. Luz, V.C. Pandolfelli, Binding additives with sintering action for high-alumina based castables, Ceram. Int. 45 (2019) 15290–15297. doi:10.1016/j.ceramint.2019.05.019.

[10] A.P. Luz, L.B. Consoni, C. Pagliosa, C.G. Aneziris, V.C. Pandolfelli, Sintering effect of calcium carbonate in high-alumina refractory castables, Ceram. Int. 44

(2018) 10486–10497. doi:10.1016/j.ceramint.2018.03.066.

[11] V.R. Salvini, P.R.O. Lasso, A.P. Luz, V.C. Pandolfelli, Nontoxic processing of reliable macro-porous ceramics, Int. J. Appl. Ceram. Technol. 13 (2016) 522–531. doi:10.1111/ijac.12521.

[12] O.H. Borges, T. Santos, V.R. Salvini, V.C. Pandolfelli, Al_2O_3–CaO macroporous ceramics containing hydrocalumite-like phases, Ceram. Int. 46 (2020) 5929–5936. doi:10.1016/j.ceramint.2019.11.046.

[13] T. Santos Jr, C.I. Pereira, R. Gonçalves, V.R. Salvini, C. Zetterström, C. Wöhrmeyer, C. Parr, V.C. Pandolfelli, Gluconate action in the hydration of calcium aluminate cements: theoretical study, processing of aqueous suspensions and hydration reactivation, J. Eur. Ceram. Soc. 39 (2019) 2748–2759. doi:10.1016/j.jeurceramsoc.2019.03.007.

[14] ASTM, C20: Standard test methods for apparent porosity, water absorption, apparent specific gravity, and bulk density of burned refractory brick and shapes by boiling water, (2015). doi:10.1520/C0020-00R15.

[15] ASTM, C133: Standard test methods for cold crushing strength and modulus of rupture of refractories, (2015). doi:10.1520/C0133-97R15.

[16] ASTM, E1875-13: Standard test method for dynamic Young's modulus, shear modulus, and Poisson's ratio by sonic resonance, (2013). doi:10.1520/E1875-13.

[17] ASTM, C1113: Standard test method for thermal conductivity of refractories by hot wire (Platinum Resistance Thermometer Technique), (2019). doi:10.1520/C1113_C1113M-09R19.

[18] B.S.M. Seeber, U.T. Gonzenbach, L.J. Gauckler, Mechanical properties of highly porous alumina foams, J. Mater. Res. 28 (2013) 2281–2287. doi:10.1557/jmr.2013.102.

[19] V.R. Salvini, V.C. Pandolfelli, D. Spinelli, Mechanical properties of porous ceramics, in: Recent Adv. Porous Ceram., InTech, 2018. doi:10.5772/intechopen.71612.

[20] P.I.B.G.B. Pelissari, R.A. Angélico, V.R. Salvini, D.O. Vivaldini, V.C. Pandolfelli, Analysis and modeling of the pore size effect on the thermal conductivity of alumina foams for high temperature applications, Ceram. Int. 43

(2017) 13356–13363. doi:10.1016/j.ceramint.2017.07.035.

[21] U.T. Gonzenbach, A.R. Studart, E. Tervoort, L.J. Gauckler, Ultrastable particle-stabilized foams, Angew. Chemie Int. Ed. 45 (2006) 3526–3530. doi:10.1002/anie.200503676.

[22] X. Mao, Processing of ceramic foams, in: Recent Adv. Porous Ceram., 1st ed., InTech, London, 2018: pp. 31–47. doi:10.5772/68104.

[23] E. Ruiz-Agudo, C. Rodriguez-Navarro, Microstructure and rheology of lime putty, Langmuir. 26 (2010) 3868–3877. doi:10.1021/la903430z.

[24] A. Irabien, A. Toquero, M.I. Ortiz, Kinetic behaviour of non-isothermal lime hydration, Chem. Eng. J. 40 (1989) 93–99. doi:10.1016/0300-9467(89)80050-4.

[25] M. Nehdi, Why some carbonate fillers cause rapid increases of viscosity in dispersed cement-based materials, Cem. Concr. Res. 30 (2000) 1663–1669. doi:10.1016/S0008-8846(00)00353-7.

[26] L. An, H.M. Chan, K.K. Soni, Control of calcium hexaluminate grain morphology in *in-situ* toughened ceramic composites, J. Mater. Sci. 31 (1996) 3223–3229. doi:10.1007/BF00354672.

[27] C. Domínguez, J. Chevalier, R. Torrecillas, G. Fantozzi, C. Domínguez, J. Chevalier, R. Torrecillas, G. Fantozzi, Microstructure development in calcium hexaluminate, J. Eur. Ceram. Soc. 21 (2001) 381–387. doi:10.1016/S0955-2219(00)00143-6.

[28] A. Bosoaga, O. Masek, J.E. Oakey, CO_2 capture technologies for cement industry, Energy Procedia. 1 (2009) 133–140. doi:10.1016/j.egypro.2009.01.020.

[29] A.L. Pereira, M.A. Reis, L.L.H.C. Ferreira, E.R. Passos, L.C. Ribeiro, M.M.M. Novo, P.M. Nakachima, Characterization of a new sintered calcium aluminate cement, Refract. Worldforum. 3 (2017) 3–6.

[30] V. Bergeron, P. Walstra, Foams, in: Fundam. Interface Colloid Sci., 2005: pp. 7.1-7.38. doi:10.1016/S1874-5679(05)80011-X.

[31] R. Wulf, G. Barth, U. Gross, Intercomparison of insulation thermal conductivities measured by various methods, Int. J. Thermophys. 28 (2007) 1679–1692. doi:10.1007/s10765-007-0278-8.

Figure Captions

Figure 1: In situ elastic modulus versus temperature for alumina-based refractory ceramics with different Ca^{2+} sources. All compositions present the same Ca^{2+} content to result in 20 wt% of CA_6 after thermal treatment. Reprinted from [9] with permission from Elsevier (license number 4714161338804).

Figure 2: Linear shrinkage and total porosity evaluated before and after firing samples with 20 wt% of theoretical amount of CA_6 at 1600ºC for 5h.

Figure 3: Pore size distribution for compositions with 20 wt% of CA_6 containing distinct Ca^{2+} sources.

Figure 4: Hot Young´s modulus of macroporous ceramic insulators containing different Ca^{2+} sources.

Figure 5: Linear shrinkage and total porosity of green and fired samples as a function of Ca^{2+} source and content.

Figure 6: SEM images for the microstructure of 20_$CaCO_3$/S71, 20_$Ca(OH)_2$/S71 and 20_CaO after firing at 1600 ºC for 5 hours. Hibonite grains are marked with H, and alumina ones with A.

Figure 7: Cold crushing strength of green and fired samples as a function of Ca^{2+} source and content.

Figure 8: Thermal conductivity (k_{eff}) of 100_$CaCO_3$/S71 and other insulating materials as a function of temperature up to 1200ºC.

Figures

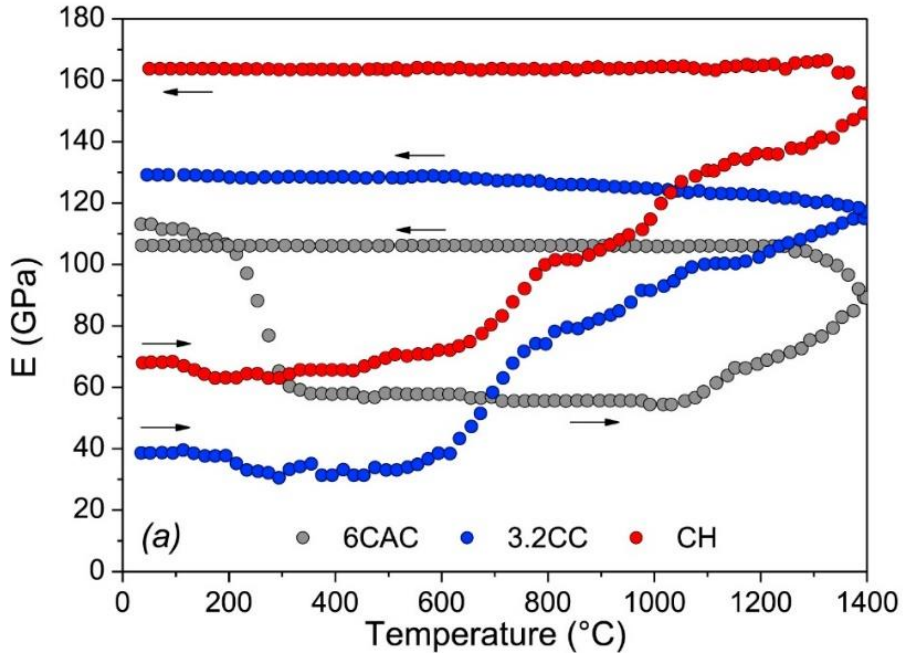

Figure 1: In situ elastic modulus versus temperature for alumina-based refractory ceramics with different Ca2+ sources. All compositions present the same Ca2+ content to result in 20 wt% of CA6 after thermal treatment. Reprinted from [9] with permission from Elsevier (license number 4714161338804).

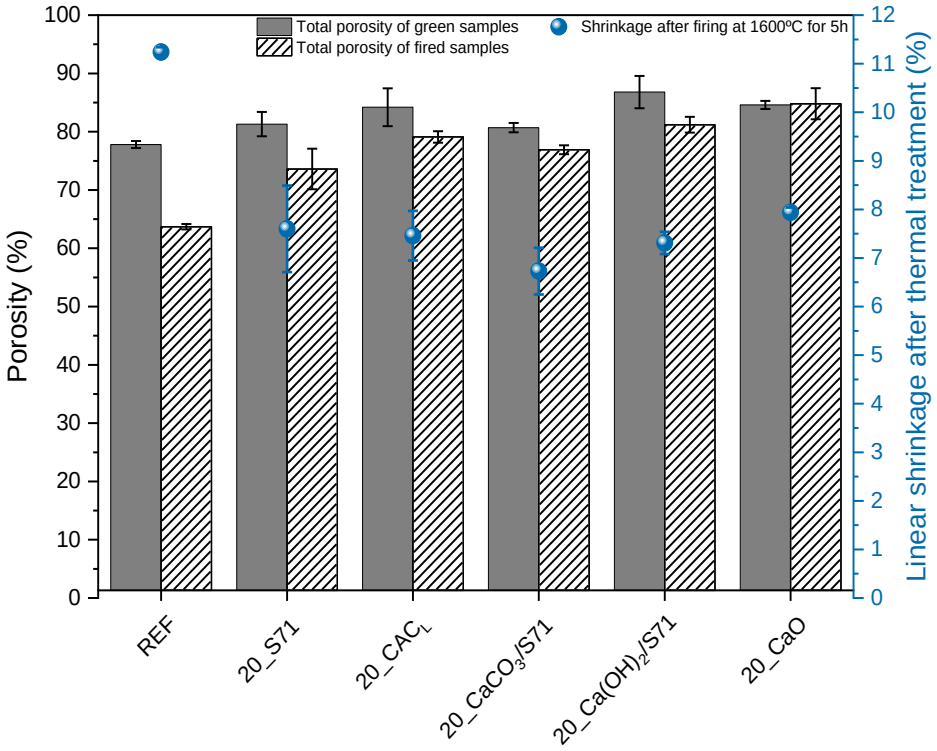

Figure 2: Linear shrinkage and total porosity evaluated before and after firing samples with 20 wt% of theoretical amount of CA6 at 1600ºC for 5h.

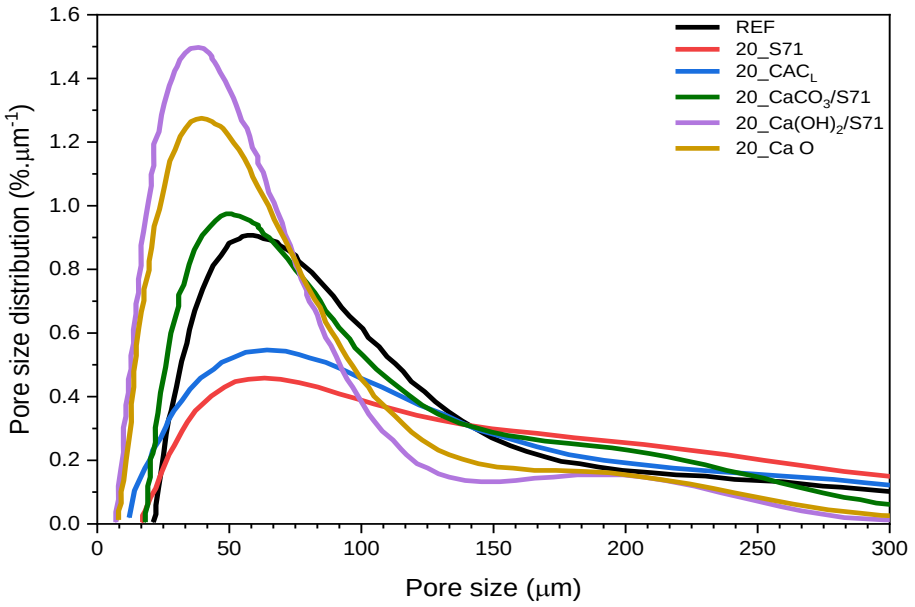

Figure 3: Pore size distribution for compositions with 20 wt% of CA6 containing distinct Ca2+ sources.

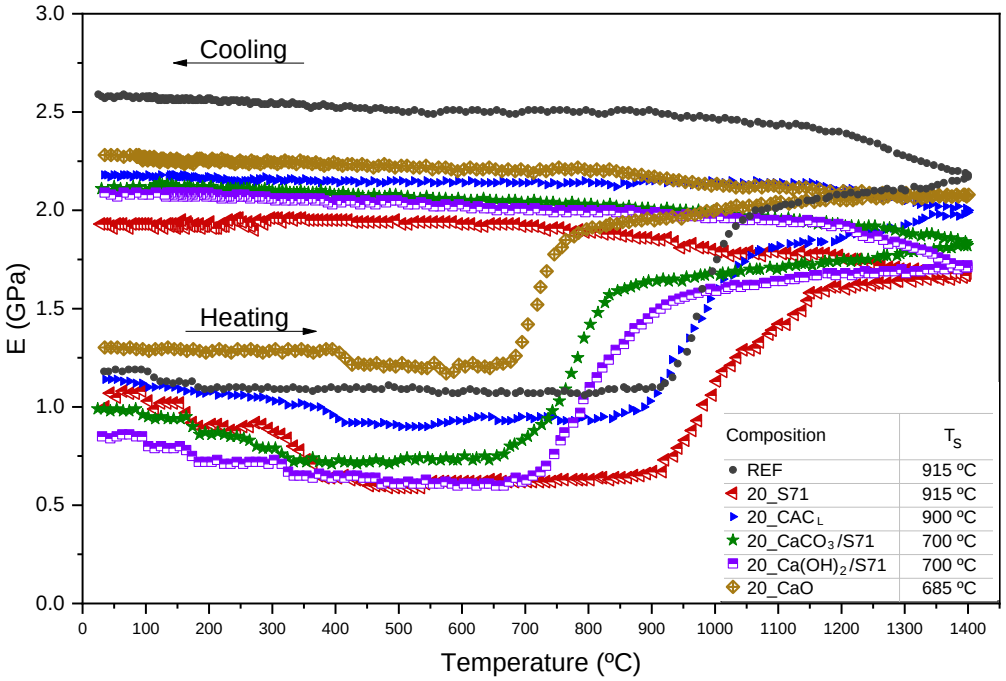

Figure 4: Hot Young´s modulus of macroporous ceramic insulators containing different Ca2+ sources.

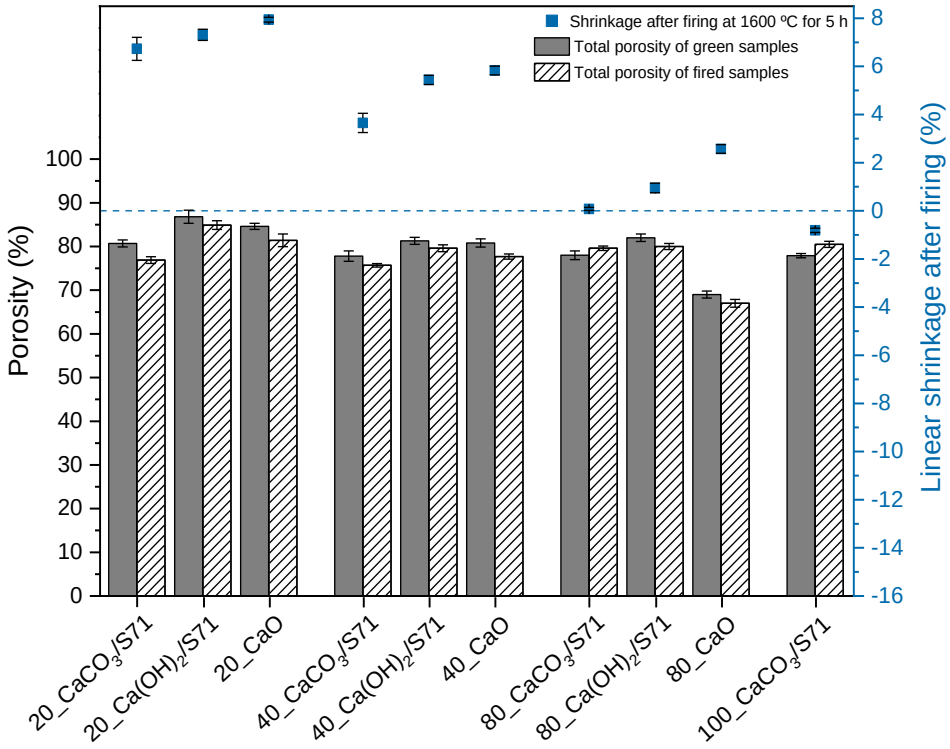

Figure 5: Linear shrinkage and total porosity of green and fired samples as a function of Ca2+ source and content.

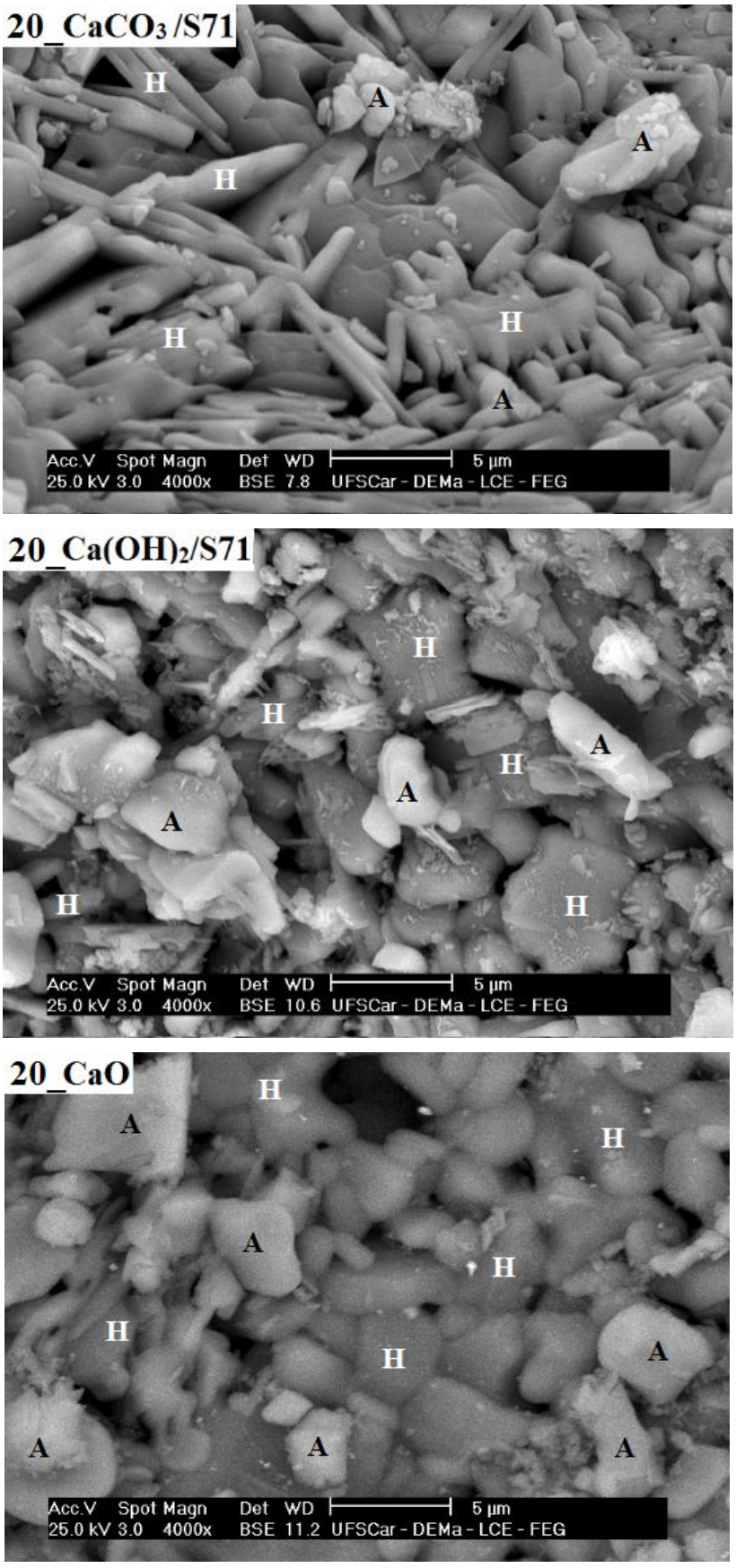

Figure 6: SEM images for the microstructure of 20_CaCO3/S71, 20_$Ca(OH)_2$/S71 and 20_CaO after firing at 1600 ºC for 5 hours. Hibonite grains are marked with H, and alumina ones with A.

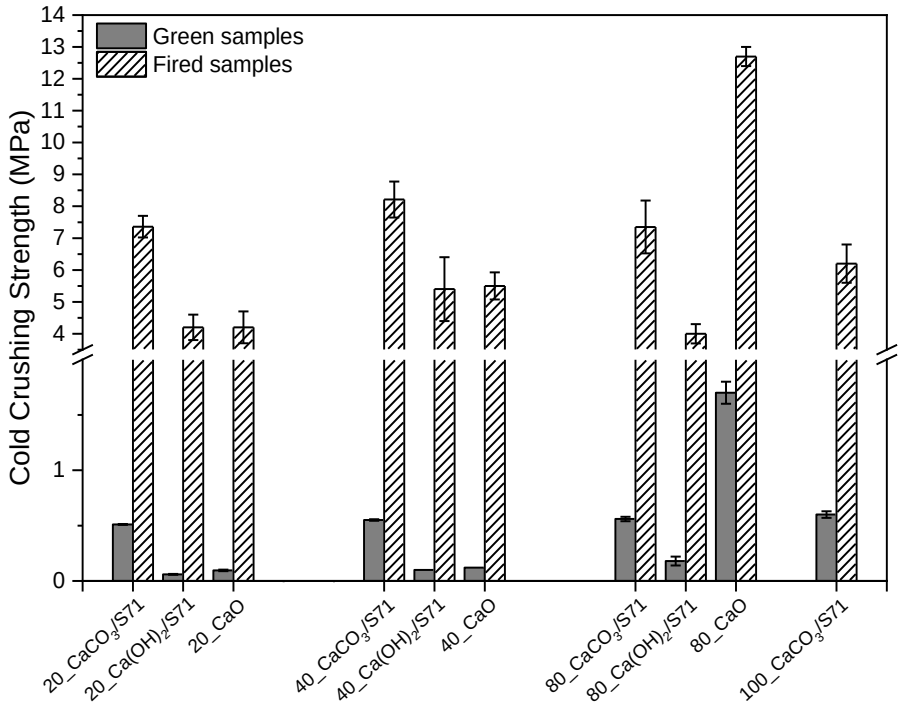

Figure 7: Cold crushing strength of green and fired samples as a function of Ca2+ source and content.

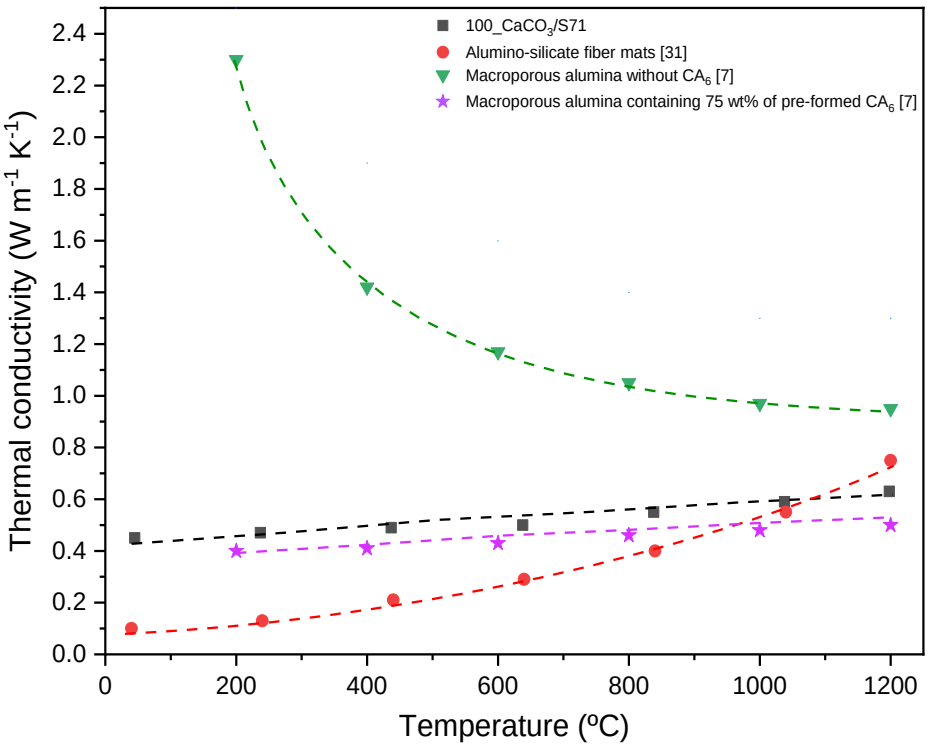

Figure 8: Thermal conductivity (keff) of 100_CaCO3/S71 and other insulating materials as a function of temperature up to 1200ºC.